Preprints, 10th IFAC International Symposium on
Advanced Control of Chemical Processes
Shenyang, Liaoning, China, July 25-27, 2018

Hybrid Online Multi-Sensor Error Detection and Functional Redundancy for Artificial Pancreas Control Systems

Jianyuan Feng*, Iman Hajizadeh *, Sediqeh Samadi*, Mert Sevil **, Nicole Hobbs, Rachel Brandt**, Caterina Lazaro***, Zacharie Maloney**, Xia Yu****, Elizabeth Littlejohn*****, Laurie Quinn******, Ali Cinar*, ****

* *Department of Chemical and Biological Engineering, Illinois Institute of Technology, Chicago, IL, USA (e-mail: jfeng12@ hawk.iit.edu).*
** *Department of Biomedical Engineering, Illinois Institute of Technology, IL, USA (e-mail: cinar@iit.edu).*

****Department of Electrical and Computer Engineering, Illinois Institute of Technology, Chicago, IL, USA (clazarom@hawk.iit.edu)*

*****Department of Control Theory and Control Engineering, Northeastern University, Shenyang, Liaoning China (xyu59@iit.edu)*

******Department of Pediatrics, University of Chicago, Chicago, IL, USA (elittlej@peds.bsd.uchicago.edu)*

*******College of Nursing, University of Illinois at Chicago, Chicago, IL, USA (lquinn18@gmail.com)*

Abstract: Sensor errors limit the performance of a supervision and control system. Sensor accuracy can be affected by many factors such as extreme working conditions, sensor deterioration and interferences from other devices. It may be difficult to distinguish sensor errors and real dynamic changes in a system. A hybrid online multi-sensor error detection and functional redundancy (HOMSED&FR) algorithm is developed to monitor the performance of multiple sensors and reconcile the erroneous sensor signals. The algorithm relies on two methods, outlier-robust Kalman filter (ORKF) and a locally-weighted partial least squares (LW-PLS) regression model. The two methods have different way of using data, ORKF is comparing current signal samples with the signal trace indicated by previous samples and LW-PLS is comparing samples in the past window with the samples from a database and uses the samples with the most similarity to build a model to predict the current signal values. The performance of this system is illustrated with a clinical case involving artificial pancreas experiments, which include data from a continuous glucose monitoring (CGM) sensor, and energy expenditure (EE) and Galvanic Skin Response (GSR) information based on wearable sensors that collect data from people with type 1 diabetes. The results indicate that the proposed method can successfully detect most of the erroneous signals and substitute them with reasonably estimated values computed by the functional redundancy system.

Keywords: Functional Sensor Redundancy, Sensor Error Detection, Kalman Filter, Locally Weighted Partial Least Squares Regression, Multi-Sensor, Signal Reconciliation

1. INTRODUCTION

Reliable sensor data is one of the most critical factors that affect the performance of monitoring and control systems. Missing signals may disrupt system operation. Outliers and large signal bias may cause the controller to calculate inaccurate values for manipulated variables, which in turn may affect the controlled variables, product quality and system safety. Sensor errors can be divided into two main categories: complete hardware failures and soft failures such as bias, drift, and outliers. (McIntosh, 2000) The solution for complete failures include fault detection, sensor replacement and/or recalibration in parallel with data reconciliation to provide "good enough" estimates for the missing data. For soft errors, the objective is to detect the error and replace the erroneous data with estimated values automatically. Many approaches have been proposed for sensor fault detection and diagnosis (FDD) and data reconciliation. Model-based methods (with first principles or data-driven models), such as Kalman estimators (Foo et al., 2013, Kobayashi and Simon, 2003, Agamennoni et al., 2011, Kobayashi and Simon, 2007), partial least squares (PLS) (Chiang et al., 2000, Kourti et al., 1995, Kim et al., 2013, Cinar and Undey, 1999, Ündey et al., 2003) and artificial neural networks (Talebi et al., 2009, Romessis and Mathioudakis, 2002) are able to detect errors by defining thresholds for measured values or their residuals and replace the erroneous signal with estimated values. Cluster-based methods such as principal component analysis based discrimination (Dunia and Joe Qin, 1998, Wang and Cui, 2005, Wang and Romagnoli, 2005, Raich and Çinar, 1997, Cinar et al., 2007) and support vector machines (Banerjee and Das, 2012, Widodo et al., 2009) aim to detect sensor errors by using a large database that includes normal and abnormal signal samples and determine the most likely cluster for the current signal. Other methods such as robust control or fault-tolerant control (Salapaka et al., 2002, McFarlane and Glover, 1990, Kendra et al., 1994) can tolerate sensor errors. A limitation of robust control is the need for prior knowledge of sensor error and its effects on the system model.

Artificial pancreas (AP) systems provide an advanced treatment for people with type 1 diabetes (T1D) by automatically regulating their blood glucose concentration (BGC). With continuous glucose monitoring (CGM), information related to BGC can be measured at a high frequency. In addition to CGM measurements, physiological information such as energy expenditure (EE) and Galvanic Skin Response (GSR) data can be used to account for the effects of physical activity that strongly affects BGC.

When a system has multiple sensors measuring different variables, the sensor signals provide the opportunity to develop functional redundancy by using models and data to detect sensor errors and reconcile erroneous signals. In previous work (Feng et al., 2017), a single sensor (CGM) version of the sensor error detection and functional redundancy (SED&FR) algorithm was reported and the AP system was used to illustrate its performance in CGM error detection and reconciliation. SED&FR uses two methods to build the prediction models, the outlier-robust Kalman filter (Ting et al., 2007, Agamennoni et al., 2011, Feng et al., 2017) (ORKF) and the locally-weighted partial least squares (Kim et al., 2013, Feng et al., 2017) (LW-PLS). This method is extended to hybrid online multi-sensor error detection and functional redundancy (HOMSED&FR) for systems with many variables. A multivariable AP which uses CGM, EE, and GSR data is used to illustrate its performance. The HOMSED&FR algorithm is integrated with an error and danger warning system (E&DWS) as a solution for hard and soft sensor errors and danger situations to improve AP safety.

2. METHODS

2.1 Model identification for multi-variable AP system

ORKF is capable to detect an outlier when the sensor signal deviation is larger than the expected sensor noise estimated by using past signal samples. The erroneous signals detected will be assigned smaller weights for updating the Kalman estimator model. LW-PLS builds a PLS model by using the signals in the historical signal database that are most similar to current signals. The fault reported by ORKF indicates that the current signal is different from the signal trace indicated by recent past values of signals, but there may not be a fault if LW-PLS find samples with similar signal behavior in the database. Conversely, if a new signal pattern does not match any type of true signal trace in the database, LW-PLS may not be able to provide the correct detection. Hence, the use of both algorithms simultaneously provides a more robust fault detection and diagnosis effort. The single sensor version of ORKF and LW-PLS described in previous work (Feng et al., 2017) has been modified to conduct FDD of MIMO systems.

In ORKF, sensor data $\boldsymbol{y}_k \in \Re^{d_1}$ can be described by Kalman filter system equations with hidden states $\boldsymbol{x}_k \in \Re^{d_2}$ where d_1 and d_2 are the dimensions of outputs (number of sensors) and state variables:

$$\boldsymbol{y}_k = \boldsymbol{C}\boldsymbol{x}_k + \boldsymbol{v}_k \tag{1}$$

$$\boldsymbol{x}_k = \boldsymbol{A}\boldsymbol{x}_{k-1} + \boldsymbol{s}_k \tag{2}$$

where $\boldsymbol{C} \in \Re^{d_1 \times d_2}$ is the observation matrix, $\boldsymbol{A} \in \Re^{d_2 \times d_2}$ is the state transition matrix, $\boldsymbol{v}_k \in \Re^{d_1 \times 1}$ is the observation noise, and $\boldsymbol{s}_k \in \Re^{d_2 \times 1}$ is the state variable noise at time step k. We assume that $\boldsymbol{v}_k$ and $\boldsymbol{s}_k$ are uncorrelated zero-mean Gaussian noise: $\boldsymbol{v}_k \sim Normal(0, \boldsymbol{R})$, $\boldsymbol{s}_k \sim Normal(0, \boldsymbol{Q})$. For the multivariable AP, the output $\boldsymbol{y}_k$ includes three measurements:

$$\boldsymbol{y}_k = [\mathrm{S}_{\mathrm{CGM},k} \quad \mathrm{S}_{\mathrm{EE},k} \quad \mathrm{S}_{\mathrm{GSR},k}]^{\mathrm{T}} \tag{3}$$

where $\mathrm{S}_{\mathrm{CGM},k}$, $\mathrm{S}_{\mathrm{EE},k}$, and $\mathrm{S}_{\mathrm{GSR},k}$ indicate signal readings of CGM, EE, and GSR at step k, respectively. The recursive model calculation procedure is described elsewhere (Feng et al., 2017). Each time a variable is updated, the ORKF will calculate an estimated value ($\hat{\boldsymbol{y}}_k^{\mathrm{ORKF}}$) that will be used in sensor error detection and data reconciliation.

For LW-PLS, the query sample ($\boldsymbol{x}_q$) and samples in the database as input ($\boldsymbol{x}_n$) contains multiple sensor signals including CGM, EE, GSR, and the insulin infusion rate. One step prediction of EE, GSR, and CGM is set as output ($\boldsymbol{y}_n$):

$$\boldsymbol{x}_n = [S'_{\mathrm{CGM},k'-\alpha}, S'_{\mathrm{CGM},k'-\alpha+1}, \dots, S'_{\mathrm{CGM},k'-1}, S'_{\mathrm{EE},k'-\alpha}, \\ \mathrm{S}'_{\mathrm{EE},k'-\alpha+1}, \dots, \mathrm{S}'_{\mathrm{EE},k'-1}, \mathrm{S}'_{\mathrm{GSR},k'-\alpha}, \mathrm{S}'_{\mathrm{GSR},k'-\alpha+1}, \dots, \\ S'_{\mathrm{GSR},k'-1}, I'_{k'-\alpha}, I'_{k'-\alpha+1}, \dots, I'_{k'-1}]^{\mathrm{T}} \tag{4}$$

$$\boldsymbol{y}_n = [S'_{\mathrm{CGM},k'}, S'_{\mathrm{EE},k'}, S'_{\mathrm{GSR},k'}]^{\mathrm{T}} \tag{5}$$

$$\boldsymbol{x}_q = [S_{\mathrm{CGM},k-\alpha}, S_{\mathrm{CGM},k-\alpha+1}, \dots, S_{\mathrm{CGM},k-1}, S_{\mathrm{EE},k-\alpha}, \\ S_{\mathrm{EE},k-\alpha+1}, \dots, S_{\mathrm{EE},k-1}, S_{\mathrm{GSR},k-\alpha}, S_{\mathrm{GSR},k-\alpha+1}, \dots, S_{\mathrm{GSR},k-1}, \\ I_{k-\alpha}, I_{k-\alpha+1}, \dots, I_{k-1}]^{\mathrm{T}} \tag{6}$$

where the prime ($'$) indicates signals from historical data in the database. The data used to build the LW-PLS database needs to be noise free, and thus a 7th order Savitzky-Golay filter (SGF) was used to filter the original CGM, EE, and GSR signals to eliminate unknown sensor noise. I denotes the insulin infusion rate. The insulin infused one hour earlier may still have an effect on BGC and CGM (Hovorka, 2006). Considering the CGM sampling time of 5 minutes, α is selected to be 12. Each time new sensor signals are provided, they will be compared with the samples in the database to find those similar samples to identify a PLS model and calculate the model prediction $\hat{\boldsymbol{y}}_k^{\mathrm{LP}}$ for sensor error detection and data reconciliation (Feng et al., 2017).

Threshold vectors $\boldsymbol{T}_{\mathrm{LW-PLS}}$ and $\boldsymbol{T}_{\mathrm{ORKF}}$ are set to determine sensor errors:

$$\boldsymbol{Err}_{\mathrm{ORKF},k} = \left\|\hat{\boldsymbol{y}}_k^{\mathrm{ORKF}} - \boldsymbol{y}_k\right\| > \boldsymbol{T}_{\mathrm{ORKF}} \tag{7}$$

$$\boldsymbol{Err}_{\mathrm{LW-PLS},k} = \left\|\hat{\boldsymbol{y}}_k^{\mathrm{LP}} - \boldsymbol{y}_k\right\| > \boldsymbol{T}_{\mathrm{LW-PLS}} \tag{8}$$

$\boldsymbol{Err}_{\mathrm{ORKF},k}$ and $\boldsymbol{Err}_{\mathrm{LW-PLS},k}$ are 3-component binary vectors, with each row equal to 1 if the condition is true and 0 if it is false. The threshold vectors are set based on the mean and standard deviation of the model prediction error (MPR) of ORKF and LW-PLS:

$$\boldsymbol{T}_{\text{LW-PLS}} = MPR_m^{\text{LW-PLS}} + MPR_d^{\text{LW-PLS}} \quad (9)$$

$$\boldsymbol{T}_{\text{ORKF}} = MPR_m^{\text{ORKF}} + MPR_d^{\text{ORKF}} \quad (10)$$

2.2 Error and danger report and signal reconciliation

The objective of a HOMSED&FR is not only to detect the sensor error, but also reconcile the erroneous sensor signals with better-estimated values. It must be sensitive to abnormal sensor readings and be able to provide accurate reconciliations. For short-duration errors such as outliers, ORKF has the advantage of fast detection and online auto-smoothing ability. For long-duration errors that require longer prediction periods, LW-PLS based on historical data is more advantageous for better prediction accuracy since no accurate prior samples are available. There are three concerns about the error reporting and signal reconciliation procedure:

1) Not all the sensor errors are automatically reconcilable. The model estimation error grows when the duration of sensor error increase. When the model is not accurate enough to give reconciled estimates of erroneous signals over an extended period, the error detection should switch from soft error to hard error and initiate an alarm, requiring for sensor calibration or sensor replacement.

2) A danger alarm should be given to guarantee the safety of the system. If either sensor signal or estimated signal indicates a safety issue of for the system (hypoglycemia or hyperglycemia for the AP) a danger alarm should be issued.

3) For a short duration error such as outliers, the erroneous sensor signals should be replaced with the estimated value with the highest performance score (model accuracy, smoothness, etc.). For a continuous sensor error, a weighted estimation could be used for erroneous signals replacement in the sense that more weight is given for the model with better-expected prediction accuracy.

There may be a large number of false positive (FP) due to variations in model accuracy, especially when a system has time-varying parameters. Nominal angle analysis (NAA) (Feng et al., 2017) is developed as a pre-check procedure to reduce the number of FP. First, sensor signals go through NAA to determine if the sensor signals are could be abnormal or the variation is due to a disturbance to the system. If NAA indicates that sensor signals are abnormal, ORKF and LW-PLS will check if the sensor signals are erroneous. If one or both of the methods report sensor error (there is a value in $\boldsymbol{Err}_{\text{ORKF},k}$ and $\boldsymbol{Err}_{\text{LW-PLS},k}$ equal to 1) or there is a missing signal, and data reconciliation is needed.

For data reconciliation, different performance scores are used for candidate selection. For CGM sensors the smoothness is the most important characteristic since glucose dynamics is relatively slow. For EE and GSR signals, large signal change is possible. For example, the human body can switch from sedentary to exercise mode such as running in few seconds and in consequence EE and GSR may increase significantly in a few sampling times.

When the first time the sensor error is detected, if the error comes from the CGM, the model estimate that has the smallest nominal angle (Feng et al., 2017) will be used to replace the erroneous sensor signal. Otherwise, the model estimate with the best accuracy at the previous sampling time will be used for the signal replacement. If there is a continuous sensor error, and initially the erroneous value is replaced by ORKF estimate, more weight should be given to LW-PLS estimate as it has better prediction accuracy for longer lasting errors:

$$S_{e,k} = 0.25Dur\hat{y}_{e,k}^{\text{LP}} + (1 - 0.25Dur)\hat{y}_{e,k}^{\text{ORKF}} \text{ if } Dur \le Dur_{\max} \quad (11)$$

where Dur is the signal error duration, with a maximum, $Dur_{\max}$. If error duration is more than $Dur_{\max}$, a hard error will be reported for sensor recalibration or replacement. If at the first time erroneous values are replaced by LW-PLS estimates, the subsequent signals of a sustained error will be replaced by $\hat{y}_{e,k}^{\text{LP}}$ until $Dur > Dur_{\max}$. The value of $Dur_{\max}$ is selected according to the prediction accuracy of LW-PLS and ORKF. For 5-steps prediction, if the average MPR is larger than 20% of the sensor signal, which is not suitable for signal reconciliation, $Dur_{\max}$ is set to 4.

The error report has four different kinds of alarms: signal missing, stuck signal, signal bias and longtime error (hard failure). An example of sensor signal reconciliation and error report including error report is illustrated in Fig. 1.

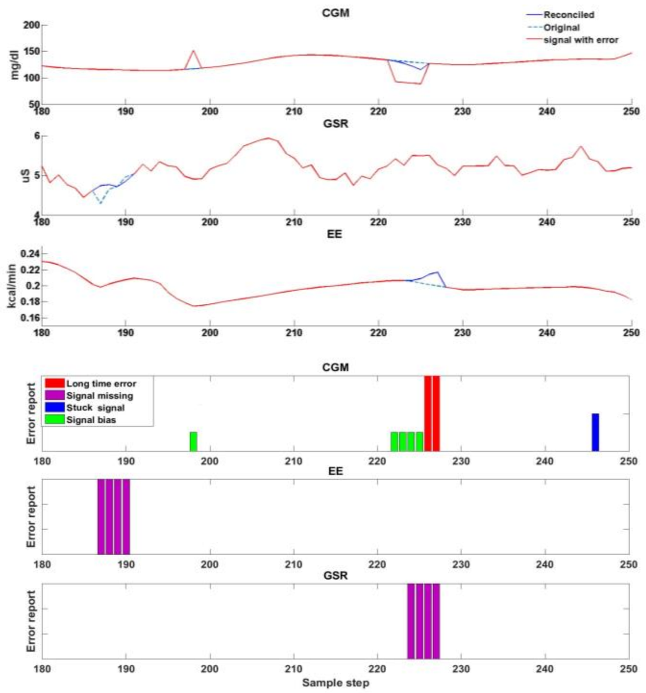

Fig. 1. Example of sensor signal reconciliation and error report

For an AP system, insulin infusion rate is calculated at every sampling time using recent values of the CGM, EE, and GSR signals. Too much insulin may cause future hypoglycemia and too little insulin may cause hyperglycemia. Hypoglycemia may cause some immediate safety issue such as coma or even death, and hyperglycemia may cause many long-term cardiovascular diseases. The normal range of glucose variations (CGM) is 70 to 180 mg/dl. A hypoglycemia alarm will be issued to consume carbohydrate if the reconciled signal is below 70 mg/dl. A hyperglycemia alarm will be issued to give a correction insulin if the glucose value is larger than 180 mg/dl. And the danger alarm system is illustrated in Fig. 2.

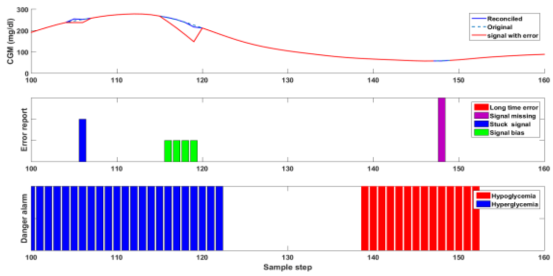

Fig. 2. Example of hypoglycemia and hyperglycemia alarm

The danger alarm is triggered (Fig. 2) even if the erroneous signal is below 180 (time 118 and 119) and signal missing (step 148). In this case, people can get immediate treatment when their BGC is in the dangerous area. The overall procedure of HOMSED&FR is illustrated in Figure 3.

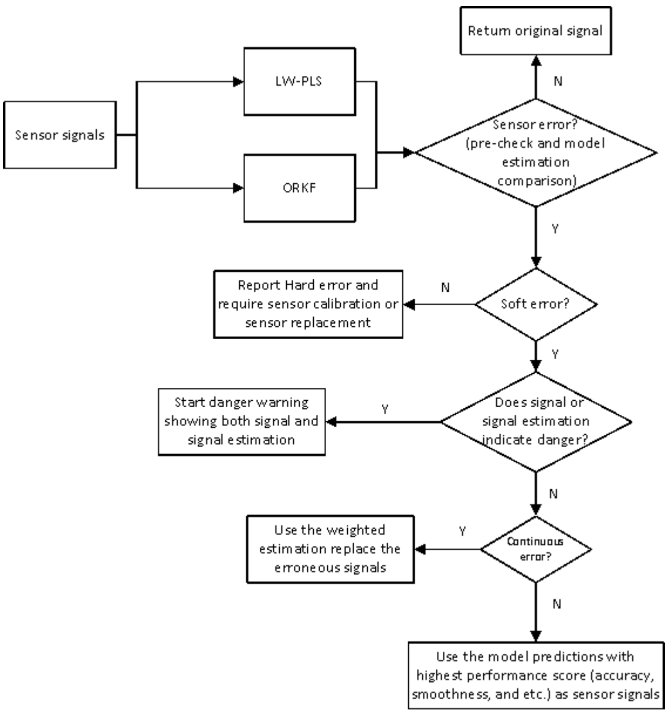

Fig. 3. Flow diagram of error report and signal reconciliation procedural of HOMSED&FR

3. RESULTS

In this case study, sensor signals collected from 16 clinical experiments with subjects with T1D who used a multivariable AP are used to illustrate the performance of the HOMSED&FR algorithm. Each experiment lasts for three days. The data include CGM sensor signals from a Dexcom G4 Platinum (Peyser et al., 2015), and EE and GSR signals from Sensewear armband (Andre et al., 2006). The sampling time for all three sensor signals is 5 minutes. In total 10,400 sets of signals were analyzed for errors. The mean and standard deviation of the three variables are listed in Table 1.

Table 1. Mean and standard deviation for the three sensors used in AP system

	CGM (mg/dl)	EE (kcal)	GSR(μS)
Mean value	141	6.74	0.485
Standard deviation	48	3.73	0.248

Since the raw sensor signal may have unknown noise, raw data are filtered by SGF to generate the noise-free data. And a sensor error generator introduces known errors to the noise-free data sets with a specified error appearance percentage (EAP) and error magnitude (M_e). EAP means the possibility of the sensor error generator adding an error to the data for each sample. Sensor errors of CGM sensor include missing signal (Eq.12), stuck signal (Eq.13), spike (Eq.14), drifts (Eq.15), step change (Eq.16), and pressure-induced sensor attenuations (PISA) (Facchinetti et al., 2016) (Eq.17). Sensor errors of EE and GSR include missing signal, stuck signal, and, spike which are the common types of error. The duration and direction of errors are noted as Du_e and Di_e respectively. The following relations are used for error generation:

$$[G_e(k), G_e(k+1) \dots G_e(k+Du_e-1)] = [\mathrm{NaN}, \mathrm{NaN}, \dots, \mathrm{NaN}] \quad \mathrm{s.t.}\ \mathrm{Du_e} \in [1,2,3,4] \tag{12}$$

$$[G_e(k), G_e(k+1) \dots G_e(k+Du_e-1)] = [G(k), G(k), \dots, G(k)] \quad \mathrm{s.t.}\ Du_e \in [1,2,3,4] \tag{13}$$

$$G_e(k) = G(k) + Di_e M_e G(k) \tag{14}$$

$$[G_e(k), G_e(k+1) \dots G_e(k+Du_e-1)] = [G(k), G(k+1), \dots, G(k+Du_e-1)] + Di_e M_e [1,2,\dots,Du_e]/Du_e \quad \mathrm{s.t.}\ Du_e \in [2,3,4,5] \tag{15}$$

$$[G_e(k), G_e(k+1) \dots G_e(k+Du_e-1)] = [G(k)+, G(k+1), \dots, G(k+Du_e-1)] + Di_e M_e G(k) \ \ s.t. Du_e \in [2,3,4,5] \tag{16}$$

$$G_e(k+t) = \begin{cases} G(k+t) - P\left(1 - \exp\left(\frac{-5t}{\tau}\right)\right) if\ t \le D/5 \\ G(k+t) + P\left(\exp\left(\frac{-5t}{\tau}\right) - \exp\left(\frac{-5t+D}{\tau}\right)\right) \\ \qquad if\ \frac{D}{5} < t < Du_e \end{cases}$$

$$\mathrm{s.t.}\ \ Du_e = D + 3\tau, \quad t \in [1, Du_e],\ P \in [10.9 \quad 48.4], D \in [3.9 \quad 21.7] \tag{17}$$

where $G_e(k)$ is the faulty sensor data generated by the sensor error generator using the original signal value $G(k)$. All types of sensor errors are added to data randomly except PISA that is only added when the subject is at resting period since PISA is usually caused by a mechanical pressure made on the sensor by the subject (e.g., sleeping position causing pressure on body region where sensor is located) inducing a temporary loss of sensitivity with consequent distortion of the CGM trace. (Bequette, 2010) All Du_e, Di_e, P, and D are randomly selected within their range (Facchinetti et al., 2016). Different magnitudes of M_e are [10% 20% 30% 40%] and the error frequency is selected as [0.1% 0.5% 1% 5%] of the total samples to illustrate the performance of the proposed system. For each combination of M_e and EPA, 10 simulations are implemented to test the HOMSED&FR algorithm. The summary of results for different M_e and EPA of different sensors are described in Tables 2 and 3, respectively.

Table 2. Summary of results for different error magnitudes

M_e(%)	Sensor	EDRS	EDRF	FN	FP	S	SRR	FDR

10	CGM	2,790	360	1,550	1,575	0.67	0.89	0.33
	EE	2,360	530	1,800	3,015	0.62	0.82	0.51
	GSR	2,470	600	1,595	1,565	0.66	0.8	0.34
20	CGM	2,980	275	1,135	1,500	0.74	0.92	0.32
	EE	2,640	545	1,630	2,935	0.66	0.83	0.48
	GSR	2,465	560	1,545	1,645	0.66	0.81	0.35
30	CGM	3,405	265	990	1,540	0.79	0.93	0.3
	EE	2,645	365	1,380	2,920	0.69	0.88	0.49
	GSR	2,430	530	1,490	1,800	0.67	0.82	0.38
40	CGM	3,450	235	945	1,435	0.8	0.94	0.28
	EE	2,955	365	1,200	2,890	0.73	0.89	0.47
	GSR	2,735	520	1,500	1,855	0.68	0.84	0.36

Table 3. Summary of results for different error appearance percentages

EAP(%)	Sensor	EDRS	EDRF	FN	FP	S	SRR	FDR
0.1	CGM	380	25	90	470	0.82	0.94	0.54
	EE	320	30	130	2,405	0.73	0.91	0.87
	GSR	175	30	80	1,950	0.72	0.85	0.9
0.5	CGM	1,325	100	460	850	0.76	0.93	0.37
	EE	1,130	160	515	2,720	0.71	0.88	0.68
	GSR	1,100	210	595	1,890	0.69	0.84	0.59
1	CGM	2,410	220	870	1,380	0.75	0.92	0.34
	EE	2,030	360	1,150	3,210	0.68	0.85	0.57
	GSR	1,970	415	1,085	1,500	0.69	0.83	0.39
5	CGM	8,510	790	3,200	3,350	0.74	0.92	0.26
	EE	7,120	1,255	4,215	3,425	0.67	0.85	0.29
	GSR	6,855	1,555	4,370	1,525	0.66	0.82	0.15

The formula for computing sensitivity (S), successful reconciliation rate (SRR), false detection ratio (FDR) are

$$S = \frac{\mathrm{EDRS+EDRF}}{\mathrm{EDRS+EDRF+FN}} \tag{18}$$

$$\mathrm{SSR} = \frac{\mathrm{EDRS}}{\mathrm{EDRS+EDRF}} \tag{19}$$

$$\mathrm{FDR} = \frac{\mathrm{FP}}{\mathrm{EDRS+EDRF+FP}} \tag{20}$$

where EDRS denotes the errors detected and reconciled successfully and EDRF denotes the errors detected but reconciliation failed. EDRS include cases during one continuous sensor error episode where the error is detected and the reconciled (estimated) value is closer to the noise-free data for sensor bias or stuck signal, and the absolute difference between the estimated value and the noise-free signal is smaller than 10% of the noise-free signal for the signal missing error. If the estimated value does not satisfy these criteria, the error is classified as EDRF. If no error is reported while there is a sensor error, it is classified as a missed error (false negative - FN), and if a sensor error is reported when no error was added to data, it is classified as error reported erroneously (false positive - FP).

4. DISCUSSION

Overall, most of the errors introduced have been detected and reconciled with better estimated values with relatively small FDR. The sensitivity and SSR increase when sensor error magnitude increases (Table 2). But FDR may not increase with the growth of sensor error magnitude since the larger magnitude of sensor error, if not detected, will affect model prediction accuracy more significantly. And when a sensor error such as step change ends and the reading returns back to real signal value, there may exist significant signal variation and the real signal may be treated as a sensor error (Fig. 2). As EAP increases, the sensitivity and FDR may increase because two or more errors may be generated close to each other. The interaction between errors will make the errors more difficult to detect. And the model based on past samples may reduce its accuracy since the models in the SED&FR system do not have enough noise-free prior data to train the model.

The sensor signal with higher variability is more difficult for error detection and signal reconciliation since there will be more FP and the model accuracy decreases when current signal values are not strongly related to previous signal values. CGM sensor signals have less variability compared with EE and GSR sensor signals (Table 1), hence have higher sensitivity and SSR and lower FDR.

At each sampling time (5 minutes) the AP system calculates an insulin infusion rate to be infused to patients. Considering the time for signal transmission, controller computation, and insulin pump execution, the computation time for HOMSED&FR need to be much smaller than 5 minutes. The computation time for this HOMSED&FR algorithm is 1.2 seconds (CPU: Intel i5-3470, RAM: 8GB, Matlab 2015a) which will not add too much computation burden to the whole AP system.

5. CONCLUSIONS

The proposed HOMSED&FR algorithm combines two methods, ORKF and LW-PLS, that together successfully detected most of the sensor errors and reconciled sensor readings for most of the detected errors with values close to the real value. The number of false alarms is relatively low. Such models improve the operation of a control system by providing reliable estimates of erroneous sensor readings. By integrating the error and danger report system, both hard and soft sensor errors are taken into consideration and improve the safety of the AP system.

ACKNOWLEDGMENTS: This work was supported by the National Institutes of Health (NIH) grant 1DP3DK101077-01 and the Juvenile Diabetes Research Foundation International (JDRF) grant 17-2013-472.

REFERENCES

AGAMENNONI, G., NIETO, J. I. & NEBOT, E. M. An outlier-robust Kalman filter. Robotics and Automation (ICRA), 2011 IEEE International Conference on, 2011. IEEE, 1551-1558.

ANDRE, D., PELLETIER, R., FARRINGDON, J., SAFIER, S., TALBOTT, W., STONE, R., VYAS, N., TRIMBLE, J., WOLF, D. & VISHNUBHATLA, S. 2006. The development of the SenseWear® armband, a revolutionary energy assessment device to assess physical activity and lifestyle. *BodyMedia Inc*.

BANERJEE, T. P. & DAS, S. 2012. Multi-sensor data fusion using support vector machine for motor fault detection. *Information Sciences,* 217**,** 96-107.

BEQUETTE, B. W. 2010. Continuous glucose monitoring: real-time algorithms for calibration, filtering, and alarms. *Journal of Diabetes Science and Technology,* 4**,** 404-418.

CHIANG, L. H., RUSSELL, E. L. & BRAATZ, R. D. 2000.

Fault diagnosis in chemical processes using Fisher discriminant analysis, discriminant partial least squares, and principal component analysis. *Chemometrics and intelligent laboratory systems,* 50**,** 243-252.

CINAR, A., PALAZOGLU, A. & KAYIHAN, F. 2007. *Chemical process performance evaluation*, CRC press.

CINAR, A. & UNDEY, C. Statistical process and controller performance monitoring. A tutorial on current methods and future directions. American Control Conference, 1999. Proceedings of the 1999, 1999. IEEE, 2625-2639.

DUNIA, R. & JOE QIN, S. 1998. Joint diagnosis of process and sensor faults using principal component analysis. *Control Engineering Practice,* 6**,** 457-469.

FACCHINETTI, A., DEL FAVERO, S., SPARACINO, G. & COBELLI, C. 2016. Modeling transient disconnections and compression artifacts of continuous glucose sensors. *Diabetes technology & therapeutics,* 18**,** 264-272.

FENG, J., TURKSOY, K., SAMADI, S., HAJIZADEH, I., LITTLEJOHN, E. & CINAR, A. 2017. Hybrid online sensor error detection and functional redundancy for systems with time-varying parameters. *Journal of Process Control,* http://dx.doi.org/10.1016/j.jprocont.2017.04.004.

FOO, G. H. B., ZHANG, X. & VILATHGAMUWA, D. M. 2013. A sensor fault detection and isolation method in interior permanent-magnet synchronous motor drives based on an extended Kalman filter. *IEEE Transactions on Industrial Electronics,* 60**,** 3485-3495.

HOVORKA, R. 2006. Continuous glucose monitoring and closed‐loop systems. *Diabetic Medicine,* 23**,** 1-12.

KENDRA, S. J., BASILA, M. R. & CINAR, A. 1994. Intelligent process control with supervisory knowledge-based systems. *IEEE Control Systems,* 14**,** 37-47.

KIM, S., OKAJIMA, R., KANO, M. & HASEBE, S. 2013. Development of soft-sensor using locally weighted PLS with adaptive similarity measure. *Chemometrics and Intelligent Laboratory Systems,* 124**,** 43-49.

KOBAYASHI, T. & SIMON, D. L. Application of a bank of Kalman filters for aircraft engine fault diagnostics. ASME Turbo Expo 2003, collocated with the 2003 International Joint Power Generation Conference, 2003. American Society of Mechanical Engineers, 461-470.

KOBAYASHI, T. & SIMON, D. L. 2007. Hybrid kalman filter approach for aircraft engine in-flight diagnostics: Sensor fault detection case. *Journal of Engineering for Gas Turbines and Power,* 129**,** 746-754.

KOURTI, T., NOMIKOS, P. & MACGREGOR, J. F. 1995. Analysis, monitoring and fault diagnosis of batch processes using multiblock and multiway PLS. *Journal of process control,* 5**,** 277-284.

MCFARLANE, D. C. & GLOVER, K. 1990. *Robust controller design using normalized coprime factor plant descriptions*, Springer.

MCINTOSH, I. B. D. 2000. *A model-based fault detection and diagnosis methodology for HVAC subsystems.* University of Wisconsin--Madison.

PEYSER, T. A., NAKAMURA, K., PRICE, D., BOHNETT, L. C., HIRSCH, I. B. & BALO, A. 2015. Hypoglycemic accuracy and improved low glucose alerts of the latest Dexcom G4 Platinum continuous glucose monitoring system. *Diabetes technology & therapeutics,* 17**,** 548-554.

RAICH, A. & ÇINAR, A. 1997. Diagnosis of process disturbances by statistical distance and angle measures. *Computers & chemical engineering,* 21**,** 661-673.

ROMESSIS, C. & MATHIOUDAKIS, K. Setting up of a probabilistic neural network for sensor fault detection including operation with component faults. ASME Turbo Expo 2002: Power for Land, Sea, and Air, 2002. American Society of Mechanical Engineers, 101-108.

SALAPAKA, S., SEBASTIAN, A., CLEVELAND, J. P. & SALAPAKA, M. V. 2002. High bandwidth nano-positioner: A robust control approach. *Review of scientific instruments,* 73**,** 3232-3241.

TALEBI, H. A., KHORASANI, K. & TAFAZOLI, S. 2009. A recurrent neural-network-based sensor and actuator fault detection and isolation for nonlinear systems with application to the satellite's attitude control subsystem. *IEEE Transactions on Neural Network,* 20**,** 45-60.

TING, J.-A., THEODOROU, E. & SCHAAL, S. 2007. Learning an outlier-robust kalman filter. *Machine Learning: ECML 2007.* Springer.

ÜNDEY, C., ERTUNÇ, S. & ÇıNAR, A. 2003. Online batch/fed-batch process performance monitoring, quality prediction, and variable-contribution analysis for diagnosis. *Industrial & engineering chemistry research,* 42**,** 4645-4658.

WANG, D. & ROMAGNOLI, J. 2005. Robust multi-scale principal components analysis with applications to process monitoring. *Journal of Process Control,* 15**,** 869-882.

WANG, S. & CUI, J. 2005. Sensor-fault detection, diagnosis and estimation for centrifugal chiller systems using principal-component analysis method. *Applied Energy,* 82**,** 197-213.

WIDODO, A., KIM, E. Y., SON, J.-D., YANG, B.-S., TAN, A. C., GU, D.-S., CHOI, B.-K. & MATHEW, J. 2009. Fault diagnosis of low speed bearing based on relevance vector machine and support vector machine. *Expert Systems with Applications,* 36**,** 7252-7261.